Metastability and dynamics of the shock-induced phase transition in iron

Jonathan C. Boettger and Duane C. Wallace
Los Alamos National Laboratory, Los Alamos, New Mexico 87545
(Received 14 June 1996)

The shock-induced α(bcc)$\rightarrow\varepsilon$(hcp) transition in iron begins at 13 GPa on the Hugoniot. In the two-phase region above 13 GPa, the Hugoniot lies well above the equilibrium surface defined by $G_\alpha = G_\varepsilon$, with G the Gibbs free energy. Also, the phase transition relaxation time τ is uncertain, with estimates ranging from <50 ns to ≈ 180 ns. Here we present an extensive study of these important aspects, metastability and dynamics, of the α-ε transition in iron. Our primary theoretical tools are (a) accurate theoretically based free energies for α and ε phases of iron and (b) accurate calculations of the wave evolution following planar impacts. We define metastable surfaces for forward and reverse transitions by the condition that the thermodynamic driving force $G_\alpha - G_\varepsilon$ is just balanced by an opposing force resulting from elastic stresses, and we calibrate the forward surface from the Hugoniot and the reverse surface from the phase interface reflection feature of shock profiles. These metastable surfaces, corresponding to $\alpha \leftrightarrow \varepsilon$ transitions proceeding at a rate of tens of nanoseconds, are in remarkable agreement with quasistatic diamond cell measurements. When the relaxation time τ is calibrated from the rise time of the $P2$ wave, our calculated wave profiles are in good agreement with VISAR data. The overall comparison of theory and experiment indicates that (a) τ depends on shock strength and is approximately $60 \rightarrow 12$ ns for shocks of $17 \rightarrow 30$ GPa, and (b) while τ expresses linear irreversible-thermodynamic relaxation, some nonlinear relaxation must also be present in the shock process in iron.
[S0163-1829(97)10305-8]

I. INTRODUCTION

In order to carry out accurate numerical calculations of dynamic processes involving inhomogeneous accelerations and deformations of metals, we must account for dynamic solid-solid phase transitions. Both the acceleration and heating of a metal depend on the changes in energy and density during a phase transition, and on the amount of work dissipated in driving the transition. This requirement of practical hydrodynamic calculations is the motivation behind the present work.

Perhaps the best studied example of a shock-induced phase transition is the $\alpha \rightarrow \varepsilon$ transition beginning at 13 GPa in iron. To facilitate discussion, let us briefly denote the major features of a plane compressive shock in iron in the order in which these features arrive at the iron free surface: EP is the elastic precursor, $P1$ is the plastic 1 wave carrying α iron to the $\alpha \rightarrow \varepsilon$ phase boundary, $P2$ is the wave in which the $\alpha \rightarrow \varepsilon$ transition proceeds, and PIR is the phase interface reflection (described in detail in Sec. V). Splitting of the main wave into $P1$ and $P2$ components, indicating presence of the phase transition, was observed by Minshall,[1] and the Hugoniot in the two-phase region was measured by Bancroft *et al.*[2] The thermodynamic equilibrium Hugoniot was calculated by Andrews,[3] and was found to differ substantially from experiment. An attempt to observe decay of the $P1$ wave led Forbes[4] to the estimate $\tau \leqslant 50$ ns, for the $\alpha \rightarrow \varepsilon$ transition relaxation time τ. Barker and Hollenbach[5] performed a series of high-resolution VISAR measurements of shock profiles in iron, from which they obtained accurate Hugoniot data and from which they estimated $\tau = 180$ ns. An extensive review of shock-induced phase transitions was published by Duvall and Graham.[6]

In this study, we have attempted to learn more about two important aspects of the shock-induced phase transition in iron: metastability and dynamics. Regarding metastability, we will present a physically based construction of the metastable path for forward and reverse transitions, and will demonstrate that this path is basically the same in shocks as in quasistatic experiments. Regarding dynamics, we will find an approximate relaxation time varying with shock strength and will then demonstrate that the VISAR data imply the presence of some nonlinearity in the relaxation process.

In Sec. II we construct and calibrate accurate theoretically based free energy functions, from which follow all the equilibrium thermodynamic functions, for α and ε phases of iron. Calculations of the following sections are based on these thermodynamic functions. In Sec. III the metastable phase transformation surface is defined for the forward transition, calibrated on the principal Hugoniot, and compared with quasistatic compression experiments. In Sec. IV it is noted that $P1$ decay does not provide a sensitive measure of τ and estimates of τ based on $P2$ rise times are presented. In Sec. V we define the metastable phase transformation surface for the reverse transition, we compare numerical wave propagation calculations with certain Barker-Hollenbach experiments, and we extract information about the phase transition rate, the nature of the PIR, and the reverse transition. Section VI summarizes the logical steps in our analysis and the corresponding conclusions on the questions of metastability and dynamics of the $\alpha \leftrightarrow \varepsilon$ transition.

II. FREE ENERGY

We will analyze the shock process to 40 GPa, which is the limit of the Barker-Hollenbach data. Figure 1 shows a portion of the iron phase diagram, containing the principal Hugoniot. On the Hugoniot, the $\alpha \rightarrow \varepsilon$ transition begins at 13

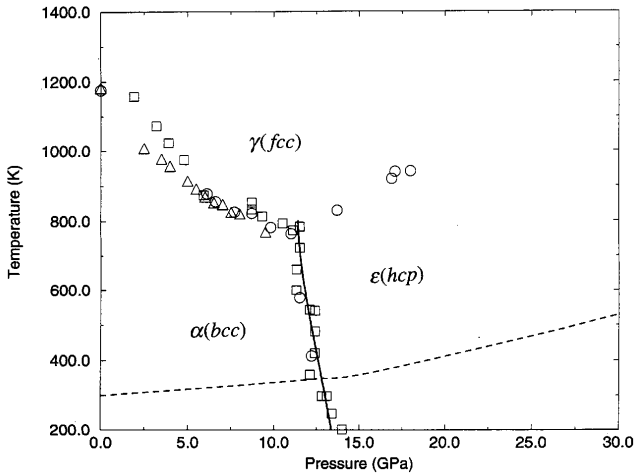

FIG. 1. Portion of the iron phase diagram. Experimental data are from Kaufman *et al.* (Ref. 24) (triangles), Bundy (Ref. 23) (circles), and Johnson *et al.* (Ref. 25) (squares). Solid line is theoretical α-ε phase boundary, and dashed line is theoretical Hugoniot.

GPa, but the two-phase region extends to around 24 GPa. Since the initial impact carries the α phase up to pressures well above 13 GPa and since the release carries the ε phase to pressures below 13 GPa, we need the free energies of both phases from room temperature to around 700 K and from 1 bar to 40 GPa.

A highly accurate free energy for crystals is based on lattice dynamics and electronic excitations. The description was presented in detail in 1972,[7] and we have since carried out many successful applications.[8–14] For a given crystal structure and for N atoms in a volume V at temperature T, the Helmholtz free energy $F(V,T)$ is written

$$F=\Phi_0+F_H+F_A+F_E, \tag{1}$$

where Φ_0 is the static lattice potential, F_H is the quasiharmonic phonon free energy, F_A is the anharmonic contribution, and F_E is the free energy due to thermal excitation of electrons from their ground state. Other thermodynamic functions, are obtained in the usual way from F; specifically, the entropy is $S=-(\partial F/\partial T)_V$, pressure is $P=-(\partial F/\partial V)_T$, internal energy is $U=F+TS$, and Gibbs free energy is $G=F+PV$. We will now describe our methods for determining each of the free energy contributions for both α and ε phases.

The quasiharmonic free energy will be needed only in its high-temperature regime, where the expansion is[7]

$$F_H=3NkT\left[-\ln\left(\frac{T}{\theta_0}\right)+\frac{1}{40}\left(\frac{\theta_2}{T}\right)^2+\cdots\right]. \tag{2}$$

The V-dependent characteristic temperatures are moments of the V-dependent phonon frequencies ω as follows:

$$\ln(k\theta_0)=\langle\ln(\hbar\omega)\rangle_{\mathrm{BZ}}, \tag{3}$$

$$(k\theta_2)^2=\tfrac{5}{3}\langle(\hbar\omega)^2\rangle_{\mathrm{BZ}}, \tag{4}$$

TABLE I. Parameters for the free energy of iron. V_{300} is the volume at 1 bar and 300 K, and θ_0, θ_2, γ_0, and $N\Gamma$ are evaluated at V_{300}.

Parameter	α (bcc)	ε (hcp)
V_{300} (cm^3/mol)	7.093	6.73
θ_0 (K)	301	261
θ_2 (K)	420	364
γ_0	1.82	2.8
$N\Gamma$ (J/mol K^2)	2.5(10^{-3})	2.5(10^{-3})
$d\ \ln\Gamma/d\ \ln V$	1.3	1.3
a^2 (K)	1135	
a^3b (J/mol)	4680	
V^* (cm^3/mol)	7.0047	6.5984
B^* (GPa)	176.64	181.5
B_1^*	4.7041	5.74
Φ^* (J/mol)	0	5533

where $\langle\cdots\rangle_{\mathrm{BZ}}$ indicates a Brillouin-zone average. The volume dependence is conveniently expressed through the Grüneisen parameters γ_n,

$$\gamma_n=-\frac{d\ \ln\theta_n}{d\ \ln V}, \quad n=0,2, \tag{5}$$

and we will use the approximations $\gamma_2=\gamma_0$ and $(\gamma_0/V)=$const, which are quite accurate for the present application. The contribution of terms denoted $+\cdots$ in Eq. (2) is negligible in the present work. Our estimates of the parameters in F_H, by means of well-developed techniques,[10–13] are listed in Table I.

From extensive analysis of experimental data, we conclude that the anharmonic free energy of most metals, including transition metals, is quite small and, in fact, is of the order of experimental error in the determination of the free energy.[10–14] The only exceptions documented at present are Cr, Mo, and W.[13] Hence we neglect F_A, which should be an excellent approximation in the present work on iron.

Thermal excitation of electrons from their ground state gives rise to the normal conduction-electron free energy F_{cond}. At the modest temperatures of interest here, F_{cond} is given by its low-temperature form

$$F_{\mathrm{cond}}=-\tfrac{1}{2}N\Gamma T^2, \tag{6}$$

and the volume dependence is expressed by a constant value of $d\ \ln\Gamma/d\ \ln V$. For α iron, Γ is obtained from low-temperature heat capacity data,[15] and $d\ \ln\Gamma/d\ \ln V$ is from band structure calculations,[13] while for ε iron both Γ and $d\ \ln\Gamma/d\ \ln V$ are from band structure calculations.[16] These parameters are listed in Table I. In addition for α iron, since the ground state is ferromagnetic, there is a magnetic contribution to the thermal excitation of electrons. From an analysis of experimental heat capacity data, Andrews[3] fitted the magnetic contribution in the form $C_{\mathrm{mag}}=bT^{3/2}/(a^2-T)$ for temperatures up to the Curie temperature $T_C=1043$ K. This corresponds to a magnetic free energy

$$F_{\rm mag}=a^3b\left[\left(1-\frac{T}{a^2}\right)\ln\left(\frac{1+\sqrt{T/a^2}}{1-\sqrt{T/a^2}}\right)-2\sqrt{\frac{T}{a^2}}+\frac{4}{3}\left(\frac{T}{a^2}\right)^{3/2}\right]. \tag{7}$$

Since the Curie temperature has virtually no pressure dependence,[17] the parameters in $F_{\rm mag}$ should be volume independent. The parameters, as determined by Andrews,[3] are listed in Table I. The total electronic free energy is

$$F_E=F_{\rm cond}+F_{\rm mag}. \tag{8}$$

The static lattice potential was determined by fitting our complete theoretical pressure $P(V,T)$ to the room-temperature compression measurements of Mao *et al.*[18,19] $\Phi_0(V)$ was written as a modification[20] of the Vinet-Ferrante-Rose-Smith (VRFS) universal form[21]

$$\Phi_0(V)=\Phi^*+\frac{4V^*B^*}{(B_1^*-1)^2}\left[1-(1+\eta)e^{-\eta}\right], \tag{9}$$

$$\eta=\tfrac{3}{2}(B_1^*-1)\left(\frac{a}{a^*}-1\right), \tag{10}$$

where a is the atomic sphere radius, given by $\frac{4}{3}\pi a^3=V/N$. The parameters in $\Phi_0(V)$ have the following significance: V^* is the volume at which Φ_0 is minimum, Φ^* is the value of Φ_0 at V^*, B^* is the bulk modulus at V^*, and B_1^* is the bulk modulus pressure derivative at V^*. Our fitted parameters for α and ε phases are listed in Table I. The data analysis of Guillermet and Gustafson[22] proved helpful in determining B^* and B_1^* for α iron. Our fitting procedure gives back the correct values of V_{300}, the volume at 1 bar and 300 K, as determined by Mao *et al.*[18,19] and listed in Table I.

Since the zero of energy is arbitrary, we set $\Phi^*=0$ for α iron. The single remaining parameter, Φ^* for ε iron, was adjusted to give α-ε phase equilibrium at 300 K and 13.0 GPa, in agreement with experiment.[23] As a check, our calculated $V_\alpha-V_\varepsilon$ at this point on the phase boundary is 0.34 $\rm cm^3/mol$, the same as experiment.[18] Our calculated α-ε phase boundary is compared with experiment[23–25] in Fig. 1.

III. PRINCIPAL HUGONIOT

The Hugoniot is the locus of thermodynamic equilibrium states, or in the case of iron it is the locus of metastable thermodynamic states, which are reached behind shocks of various strengths, starting from a given initial state. The principal Hugoniot starts from room temperature and pressure, taken here as 300 K and 1 bar. To calculate a point on the Hugoniot, we generate a plane compressive wave by applying a constant-velocity boundary condition and then read the thermodynamic variables in the time-independent state far behind the wave front. This Hugoniot state is correct regardless of the nature of the propagating wave, in particular whether or not the wave is steady, and the Hugoniot state is independent of the rates of irreversible processes which occur in the wave front.

The Hugoniot state depends entirely on the continuum mechanic laws of conservation of mass, momentum, and energy, and on the thermodynamic equilibrium or metastable surface. To define this surface we first assume pressure and temperature equilibrium between the α and ε phases, at all times and locations:

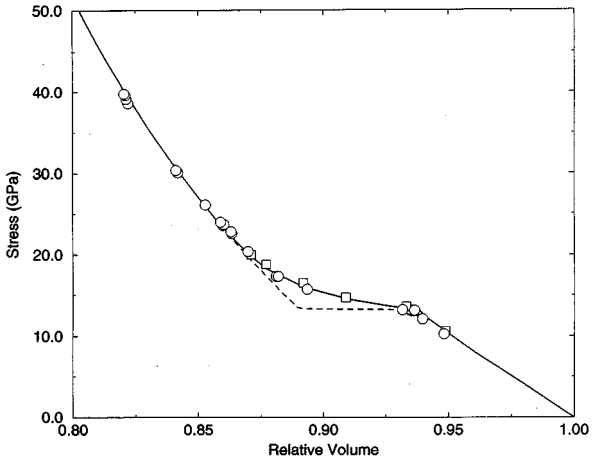

FIG. 2. Iron Hugoniot. Experimental data are from Bancroft *et al.* (Ref. 2) (squares), and Barker and Hollenbach (Ref. 5) (circles). Dashed line is theoretical equilibrium Hugoniot, and solid line is theoretical metastable Hugoniot.

$$P_\alpha=P_\varepsilon=P, \quad T_\alpha=T_\varepsilon=T. \tag{11}$$

We then define λ as the mass fraction of the ε phase present, and so $0\leqslant\lambda\leqslant1$, and the extensive thermodynamic functions are expressed as sums of the α and ε contributions:

$$V=(1-\lambda)V_\alpha+\lambda V_\varepsilon, \tag{12}$$

with similar expressions for U, S, and G.

The experimental wave profiles exhibit an elastic precursor which corresponds to a yield strength of approximately 3 kbar in α iron.[26] Beyond this, the experiments tell us nothing about how the yield strength varies with plastic strain or strain rate, or what happens to the yield strength during the phase transition. Unfortunately, we are not able to shed any light on these important questions in the present work. However, we feel it is important to include the elastic precursor in our calculations, and so we do this with a simple elastic-plastic model with a constant yield strength $y=3$ kbar. Hence our Hugoniot states are characterized by a normal stress σ and the pressure P, which are related by

$$\sigma=P+\tfrac{4}{3}y. \tag{13}$$

The equilibrium phase boundary satisfies $G_\alpha(P,T)=G_\varepsilon(P,T)$. This determines a line in P,T space or a surface on which λ varies between 0 and 1 in V,T space. If we assume iron moves across this surface as the phase transition proceeds within the shock, we find the ''equilibrium'' Hugoniot shown in Fig. 2. The experimental Hugoniot, also shown in Fig. 2, is far from the equilibrium Hugoniot in the two-phase region from 13 to around 24 GPa. This discrepancy was revealed by the calculations of Andrews.[3]

Clearly, then, the mixed-phase Hugoniot states in iron lie on a metastable surface whose lifetime is long compared to the time of the shock experiments and whose pressure is

significantly higher than that on the equilibrium surface. In fact, such behavior is not unique, since a similar metastable Hugoniot describes the α-quartz→stishovite transition in silica[27] and the related phase transition in granite.[28]

Let us consider the entire metastable two-phase surface in iron, not limited to Hugoniot states. We concentrate first on the forward $\alpha \rightarrow \varepsilon$ transition and denote by λ_m the metastable states reached by driving the transition to partial completion. Since the transition proceeds out of equilibrium, the thermodynamic driving force is $\Delta G = G_\alpha - G_\varepsilon$. However, because of the large volume change $\Delta V/V \approx 0.05$, an increment of the transition process is expected to generate stresses which oppose further transformation. Balancing forward and reverse forces implies $d\lambda_m \propto d\Delta G$. But $d\lambda_m$ should also be proportional to the amount of α iron present, which is $1-\lambda_m$, and so we conclude

$$d\lambda_m \propto (1-\lambda_m) d\Delta G. \tag{14}$$

Integrating this gives

$$\lambda_m = 1 - \exp[(A_F - \Delta G)/B_F], \tag{15}$$

where A_F plays the role of an activation energy and B_F measures the energy scale of the opposing forces, with $B_F > 0$. The forward transition proceeds when $A_F - \Delta G < 0$. The reverse transition will be considered in Sec. V. We note that the form (15) for λ_m was obtained empirically by Forbes[4] from a direct analysis of Hugoniot data.

We can calibrate the metastable surface by fitting Eq. (15) to the experimental Hugoniot. The fit to experiment can be made quite good, as shown in Fig. 2, with the corresponding parameters for the forward transition:

$$A_F = 0,$$

$$B_F = 642 \ \text{J/mol}. \tag{16}$$

Since we adjusted the free energies to achieve $G_\alpha = G_\varepsilon$ at the equilibrium phase boundary, the fitted value $A_F = 0$ means the shock transition begins at the equilibrium phase boundary. Our calculated results for thermodynamic data on the Hugoniot are listed in Table II.

In recent years the α-ε transition has been extensively studied in diamond-cell experiments at room temperature.[29–31] Even in these ''quasistatic'' experiments, the phase transition does not proceed on the equilibrium surface. The pressure spread from beginning to end of the transition depends strongly on the shear strength of the stress-transmitting medium, while the midpoints of the forward-reverse hysteresis lie consistently near 13 GPa.[30] The forward-transition metastable surface we find from the shock Hugoniot is remarkably similar to that found in nearly hydrostatic diamond-cell measurements.[31] To make this comparison we solved λ_m $(\Delta G(P,T))$, given by Eq. (15), for $P(\lambda_m)$ at $T = 300$ K, with the results shown in Fig. 3. The small amount of ε phase seen in the diamond cell below 13 GPa is not apparent in our λ_m curve; indeed, Barker made a special study and found no evidence for partial transformation in shocks below 13 GPa.[32]

TABLE II. Calculated data on the principal Hugoniot. u_p is particle velocity, $V^\alpha_{300} = 7.093$ cm^3/mol, and σ is normal stress.

u_p (km/s)	V/V^α_{300}	σ (GPa)	T (K)	λ_m
0.10	0.9803	4.00	313	0.000
0.20	0.9606	7.99	328	0.000
0.30	0.9417	12.20	345	0.000
0.323[a]	0.9378	13.22	350	0.000
0.33	0.9346	13.32	349	0.060
0.35	0.9260	13.67	349	0.218
0.39	0.9102	14.48	352	0.485
0.45	0.8921	15.98	364	0.765
0.52	0.8772	18.26	388	0.927
0.57	0.8693	20.23	410	0.973
0.65	0.8583	23.81	450	0.995
0.72	0.8496	27.23	489	0.999
0.80	0.8394	31.37	542	1.000
0.87	0.8307	35.18	595	1.000
0.95	0.8213	39.75	665	1.000

[a]Hugoniot point atop the $P1$ wave.

IV. PHASE TRANSITION RELAXATION TIME

The relaxation time for the shock driven $\alpha \rightarrow \varepsilon$ transition has been estimated from the decay of the $P1$ wave. Forbes[4] used a streak camera to observe the $P1$ wave for 20 GPa shocks emerging from samples 1–6 mm thick, and finding no $P1$ decay, he concluded the relaxation time is $\leqslant 50$ ns. $P1$ decay was observed in the more sensitive VISAR experiments of Barker and Hollenbach,[5] who fitted their results to the theory of Horie and Duvall[33] and found a relaxation time of 180 ns. The theory of Horie and Duvall accounts for $P1$ decay caused by the phase transition going on at the peak of the $P1$ wave. However, there exists a second source of $P1$ decay, which can be of either sign, resulting from processes going on in regions behind the $P1$ wave and propagating

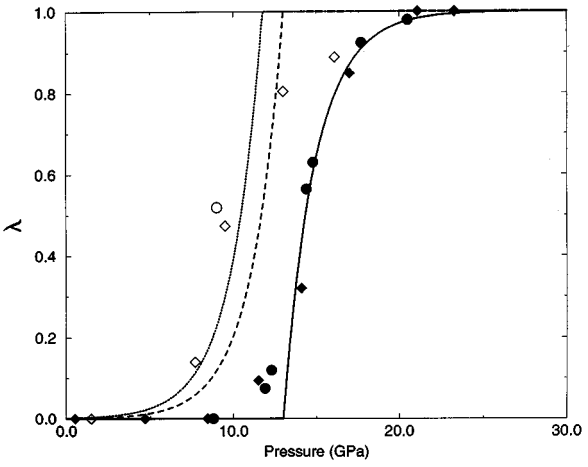

FIG. 3. λ vs P for forward and reverse transitions at 300 K. Symbols are diamond-cell data of Taylor *et al.* (Ref. 31) with solid (open) symbols corresponding to increasing (decreasing) pressure. Solid line is forward transition metastable surface, and dashed and dotted lines show reverse transition metastable surface with $A_R = 0$ and $A_R = 419$ J/mol, respectively.

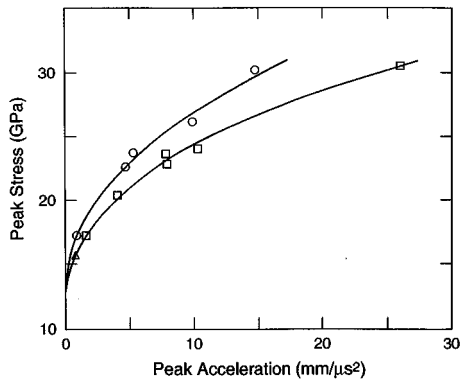

FIG. 4. Peak shock stress vs peak free surface acceleration in the $P2$ wave. Barker-Hollenbach (Ref. 5) data are for specimen thickness 3.11 mm (triangle), 6.3 mm (squares), and 16–19 mm (circles). Lines are graphical fits for thick and thin specimens.

stress increments forward. The complete equation for the rate of change of stress atop the $P1$ wave has been given by Johnson,[34] wherein the second contribution to $P1$ decay is proportional to the particle acceleration atop the $P1$ wave. We estimated this contribution for experiment 19 of Barker and Hollenbach[5] by evaluating the free surface acceleration from the slope shown in their Fig. 9 and found that the omitted term is completely dominant for this particular experiment. The result indicates, for the range of experimental parameters covered by Barker and Hollenbach, that $P1$ decay does not provide a sensitive way to determine τ.

Since the phase transformation process occurs in the front of the $P2$ wave, then $P2$ rise times should give the most direct information about the transformation rate. Let us ask whether or not the $P2$ rise times are well resolved in the measurements of Barker and Hollenbach. Fortunately, Barker and Hollenbach had the foresight to tabulate the peak free-surface acceleration in their $P2$ waves. When these peak accelerations are graphed as a function of shock stress, they lie on a single curve with moderate scatter. On closer examination, the peak accelerations are found to define two separate curves, each with very little scatter, one for samples around 6 mm thick and another for samples 16–19 mm thick. This result is shown in Fig. 4, where the smooth curves were made to pass through zero acceleration at a shock stress of 13.2 GPa and where the one sample of around 3 mm thickness lies on the curve for the 6-mm samples. Two important conclusions follow from Fig. 4.

(a) Rise times of the $P2$ waves are well resolved by the measurements of Barker and Hollenbach.

(b) The $P2$ waves are not steady for the thin specimens, since at a fixed stress their rise times are still increasing with distance traveled.

Between the initial and final states of a shock, the material passes through nonequilibrium states. In the $\alpha \rightarrow \varepsilon$ transition, the iron passes through states which lie above the metastable Hugoniot curve (see Fig. 2). From the principles of linear irreversible thermodynamics, there should exist a driving force which is linear in the distance of the iron from the metastable surface and which drives the transition in such a way as to move the iron toward the metastable surface. This is expressed in the relation $\dot{\lambda}=(\lambda_m-\lambda)/\tau$, where τ is the relaxation time. But this relation is not yet unique, since the distance from the metastable surface depends on the direction along which $\lambda_m-\lambda$ is evaluated. Since the nonequilibrium driving force is proportional to $\Delta G(P,T)$, then the distance $\lambda_m-\lambda$ should be measured at constant P and T, and so we write

$$\frac{d\lambda}{dt}=\frac{\lambda_m(P,T)-\lambda(P,T)}{\tau}. \tag{17}$$

We refer to this form as ''linear relaxation'' and note in the most general case that τ can depend on the state variables, e.g., $\tau=\tau(P,T)$. The result (17) differs from previous models, in that Horie and Duvall[33] measured $\lambda_m-\lambda$ at constant V and T, Andrews[3] measured $\lambda_m-\lambda$ at constant V and U, and both used $\lambda_{\rm eq}$ in place of λ_m.

If we are willing to approximate the $P2$ waves as steady, we can estimate τ directly from the $P2$ rise times. Note that the steady-wave approximation is on the order of neglecting the difference between the two curves in Fig. 4. For a steady $P2$ wave, the material path in the wave front, i.e., the Rayleigh line, is a straight line on the Hugoniot diagram of Fig. 2, from the start of the two-phase region to the final Hugoniot state. For this process we can approximate the integral of Eq. (17) for $\dot{\lambda}$ to obtain a Rayleigh-line average of λ in terms of τ. But, also, since a given $P2$ wave carries λ from 0 to λ_m, the mean value of $\dot{\lambda}$ is roughly λ_m/t_2, where t_2 is the $P2$ rise time. Equating these two averages of $\dot{\lambda}$ yields the approximate relation

$$\tau \approx t_2\left[\frac{1}{\lambda_m}-\frac{1}{2}+\frac{1}{\ln(1-\lambda_m)}\right]. \tag{18}$$

The rise time can be expressed

$$t_2=\Delta u_2/\alpha_2, \tag{19}$$

where Δu_2 is the increase in particle velocity across the $P2$ wave, which we evaluate from the steady-wave jump condition, and α_2 is the peak particle acceleration in the $P2$ wave, approximately half the peak free surface acceleration.

Data entering the calculation of τ, taken from Barker and Hollenbach,[5] and from our own determination of λ_m, are listed in Table III, and values of τ are graphed in Fig. 5. While peak $P2$ accelerations vary by a factor of 40, the estimated relaxation times vary by only a factor of 5. Moreover, considering τ a function of P and T means τ can depend on the peak shock stress, and this dependence accounts for most of the variation in τ, as shown in Fig. 5. Nevertheless, Fig. 5 still shows a dependence of τ on specimen thickness, which corresponds to the same dependence shown in Fig. 4 for the peak accelerations and which is related to the nonsteady character of the $P2$ waves, at least for the thin specimens. Therefore, to eliminate the steady-wave approximation, we carried out accurate numerical wave-evolution calculations to compare with several of the experiments of Barker and Hollenbach. The results of these calculations are presented in the next section.

V. WAVE PROFILE ANALYSIS

We used a one-dimensional hydro code to calculate impact experiments identical to the experiments of Barker and Hollenbach.[5] Our initial data consisted of specimen and im-

TABLE III. Evaluation of the relaxation time from the steady-wave approximation, applied to the experiments of Barker and Hollenbach.

Experiment number	Peak stress (GPa)	α_2 (mm/μs^2)	t_2 (ns)	τ (ns)
1	17.3	0.76	209	32
2	20.4	2.00	114	29
3	17.3	0.43	386	59
4	22.6	2.33	121	34
5	23.6	3.93	75	23
6	30.4	13.0	32	12
7	23.7	2.645	116	36
8	30.1	7.4	58	21
17	24.0	5.15	58	19
18	22.8	3.95	70	20
19	26.1	4.95	71	24
20	15.7	0.335	290	29

pactor thicknesses, the impact velocity, and the initial thermodynamic state (1 bar and 300 K). For all calculations presented here, cell size was 4 μm and time step was 0.1 ns. Calculations without artificial viscosity showed very small reverberations atop the $P1$ wave, and these reverberations left a very small amount ($\sim$0.1%) of iron in the ε phase. Since this appearance of ε iron in the $P1$ wave is physically incorrect, we included a very small linear plus quadratic artificial viscosity to eliminate these reverberations. We verified that the artificial viscosity has no significant affect upon our ultimate determination of physical properties of iron. As mentioned in Sec. III, we included elastic-plastic behavior with a constant yield strength and with complete dissipation of plastic work. The metastable surface for the forward transition is expressed in Eq. (15), the forward transition proceeds when $A_F-\Delta G<0$, and the parameters were determined by fitting the Hugoniot. We construct the reverse transition metastable surface from the same arguments used for the forward transition: The thermodynamic driving force ΔG is balanced by opposing stresses created by the

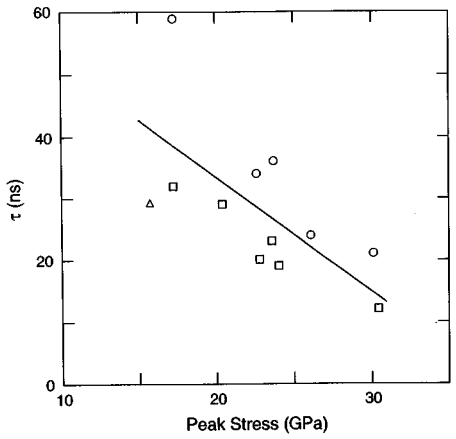

FIG. 5. Approximate $\alpha\rightarrow\varepsilon$ relaxation times from Eq. (18) vs peak shock stress. Symbols represent specimen thickness as in Fig. 4, and the line is a rough representation of the points.

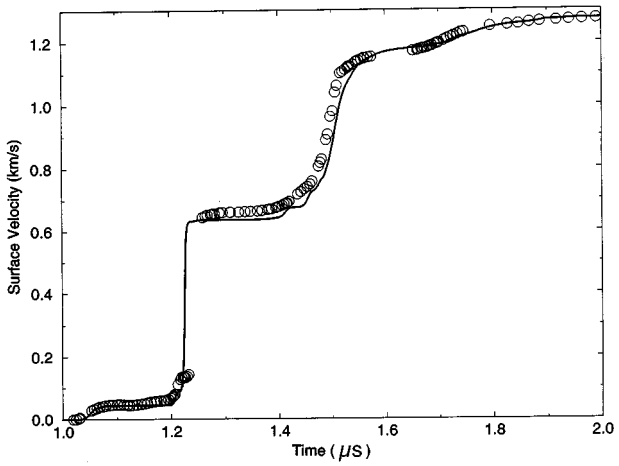

FIG. 6. Free surface velocity vs time for experiment 5: Circles are VISAR data of Barker and Hollenbach (Ref. 5), and line is our calculation. In order of their arrival at the free surface, the four main waves are the EP, $P1$, $P2$, and PIR.

transition process, implying $d\lambda_m\propto d\Delta G$, and $d\lambda_m$ is also proportional to the amount of ε phase present, which is λ_m, so that

$$d\lambda_m\propto\lambda_m d\Delta G. \tag{20}$$

This integrates to

$$\lambda_m=\exp[(\Delta G-A_R)/B_R], \tag{21}$$

where the reverse transition proceeds when $\Delta G-A_R<0$ and where the parameters will be determined by our wave profile analysis. For both forward and reverse transitions, the transition rate was expressed by the linear-relaxation equation (17), where the relaxation time τ was considered adjustable, but was held constant for the entire calculation of a single experiment.

In experiment 5 of Barker and Hollenbach, the specimen was 6.314 mm thick, the impact velocity was 1.292 km/s, and the peak stress was 23.6 GPa. Our calculated free surface velocity is compared with the VISAR data in Fig. 6, where the following characteristics of all our calculations are illustrated.

(1) The EP arrival time, which depends primarily on our adiabatic elastic moduli, agrees with experiment to 0.5% or better.

(2) The EP free surface velocity is in good agreement with experiment.

(3) The height of the $P1$ wave, which depends on the Hugoniot stress at which the transition begins, is in excellent agreement with experiment.

(4) The calculated $P1$ wave is narrower and travels faster than experiment. These discrepancies, which presumably result from our failure to account for rate-dependent plasticity, are of no concern in our analysis of the phase transition process.

(5) Reflections of the EP, seen ahead of $P1$ and $P2$, are in qualitative agreement with the experimental profiles.

(6) Arrival times and shapes of $P2$ and the PIR are in excellent agreement with experiment. Note that this part of

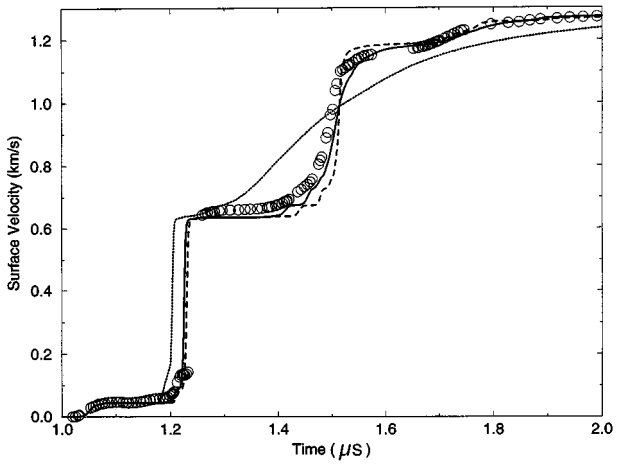

FIG. 7. Free surface velocity vs time for experiment 5 of Barker and Hollenbach (Ref. 5) (circles), compared with calculations for $\tau=1$ ns (dashed line), $\tau=30$ ns (solid line), and $\tau=180$ ns (dotted line).

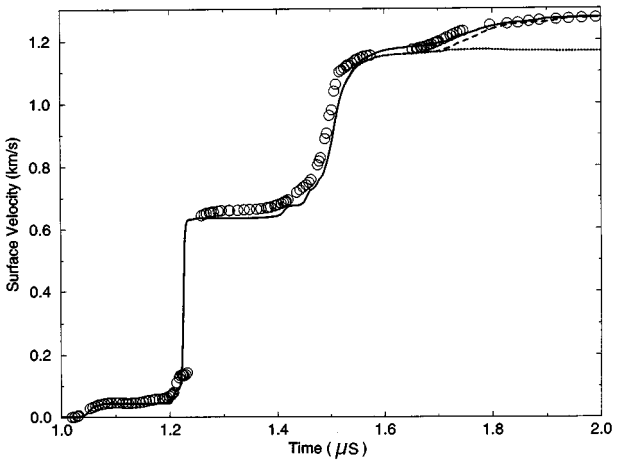

FIG. 8. Free surface velocity vs time for experiment 5 of Barker and Hollenbach (Ref. 5) (circles), compared with calculations for $A_R=0$ (solid line), $A_R=419$ J/mol (dashed line), and $A_R=\infty$ (dotted line).

the calculated profiles depends on the complete thermodynamics of both phases and, also, on the parameters in the phase transition process, as described below.

(7) The final free surface velocity is practically identical to the VISAR data. This is not a trivial result since, as shown below, this final velocity is controlled by reverse transformation in the PIR.

The rise time of the $P2$ wave is strongly influenced by the relaxation time τ. Calculations for experiment 5, with $\tau=1$, 30, and 180 ns, are compared with VISAR data in Fig. 7. Though the entire $P2$ and PIR structures vary with τ, if we concentrate on the $P2$ rise time, we conclude that $\tau=30$ ns gives the best agreement with experiment. When τ is fixed, the PIR depends on the metastable surface $\lambda_m(\Delta G)$ for the reverse transition, Eq. (21). However, we have consistently found practically no sensitivity to B_R, and so we set this parameter equal to the forward transition value,

$$B_R=B_F=642 \text{ J/mol}. \tag{22}$$

Calculations for experiment 5, with $A_R=0$ and 419 J/mol, are compared with VISAR data in Fig. 8, and we conclude that optimal agreement with the PIR arrival time and shape corresponds to A_R between these values and probably closer to the smaller value. The parameter A_R determines at what pressure the reverse transition begins, with the following correspondence at 300 K:

$$A_R=0 \text{ J/mol}\Rightarrow P_R=13.0 \text{ GPa},$$

$$A_R=419 \text{ J/mol}\Rightarrow P_R=11.8 \text{ GPa}. \tag{23}$$

The reverse transition paths at 300 K, corresponding to these two values of A_R, are in qualitative agreement with diamond cell data, as may be seen from Fig. 3.

The origin of the PIR was explained by Barker and Hollenbach briefly as follows. First, the $P1$ reaches the free surface and sends back a release wave. This release encounters the oncoming $P2$ and reduces the $P2$ stress by 13 GPa, so that the residual $P2$ is not strong enough to drive the $\alpha\rightarrow\varepsilon$ transition. This leaves a phase interface in the specimen, ahead of which is α iron and behind which is ε iron. Now the residual $P2$ reaches the free surface and sends back a release wave. When the $P2$ release enters the ε phase, it drives the $\varepsilon\rightarrow\alpha$ transition, resulting in a mismatch of material properties at the phase interface and causing part of the $P2$ release to be reflected back toward the free surface as a recompression, the PIR.[5]

Our calculations verify this origin of the PIR and add some interesting refinements. First, the reverse transformation process indeed generates a small pressure pulse, which then propagates as the PIR. Since the period of time over which this pressure pulse is generated depends on τ, the origination time of the PIR, and, hence, the free surface arrival time of the PIR, also depend on τ. This behavior is shown in Fig. 7, where increasing τ is seen to delay the PIR arrival at the free surface. It is also clear why the arrival time and shape of the PIR depend sensitively on the pressure at which the reverse transition begins, so that the PIR gives us a rather accurate determination of the parameter A_R, as shown in Fig. 8. Finally, by taking a large positive value for A_R, the reverse transition is prohibited, the ε phase behind the phase interface is frozen in, and the PIR disappears completely, also as shown in Fig. 8. This suggests another way of seeing the role of the PIR in the shock process in iron. Since experiment 5 is a symmetric impact of two pieces of α iron, in the absence of any phase transition, the free surface velocity should reach the impact velocity of 1.292 km/s. Except for dissipative losses, the same free surface velocity should be reached when the phase transition is present, as long as the final phase is α, the same as the initial phase. Hence the role of the PIR is to increase the free surface velocity to its correct final value, when the iron is returned from ε to its initial phase α. But when the ε phase is frozen in, the free surface velocity cannot reach the impact velocity, since energy is locked into the higher energy ε phase (Fig. 8).

In a series of articles,[35–38] Nigmatulin and co-workers presented a theoretical study of the kinetics of the shock-induced phase transition in iron, and ultimately they calculated[38] the profile of experiment 5 of Barker and

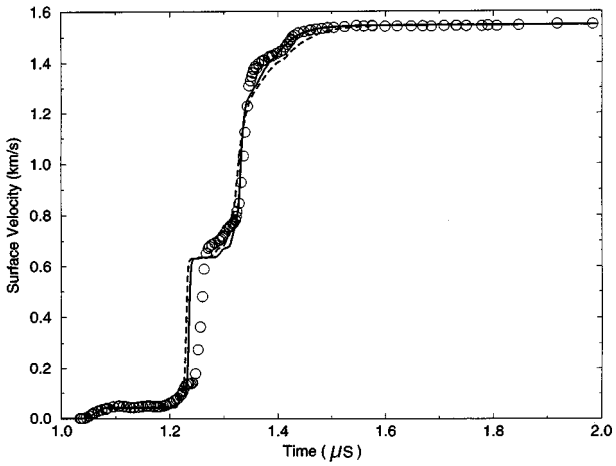

FIG. 9. Free surface velocity vs time for experiment 6 of Barker and Hollenbach (Ref. 5) (circles), compared with calculations for $\tau=15$ ns (solid line) and $\tau=30$ ns (dashed line).

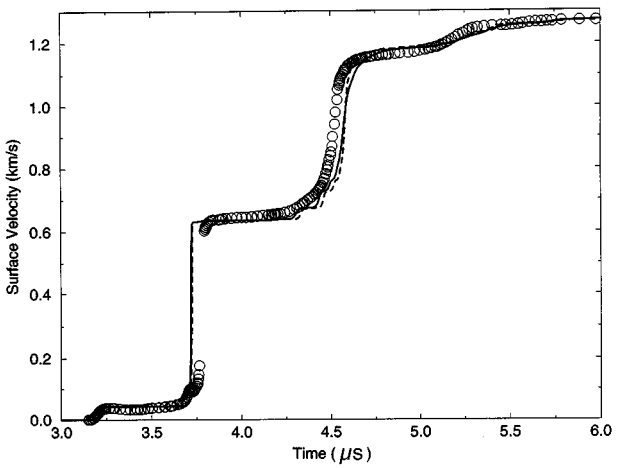

FIG. 10. Free surface velocity vs time for experiment 7 of Barker and Hollenbach (Ref. 5) (circles), compared with calculations for $\tau=30$ ns (dashed line) and $\tau=60$ ns (solid line).

Hollenbach.[5] Since Nigmatulin and co-workers used rate-independent plasticity, their $P1$ rise time, which agrees with experiment, is controlled by artificial viscosity. But this same rather large artificial broadening also contributes to their $P2$ rise time and, hence, obscures the interpretation of their phase transition rate parameters. Also, Nigmatulin and co-workers[35–38] set the irreversible driving force proportional to the distance from the equilibrium surface, as other workers have done.[3,33] Wave calculations based on this condition yield the equilibrium Hugoniot of Fig. 2, not the metastable (experimental) Hugoniot. Since the phase transition process stops at $\lambda=\lambda_m$, the net irreversible driving force is actually proportional to the distance from the metastable surface, as shown in Eq. (17).

Experiment 6 of Barker and Hollenbach is a thin specimen, like experiment 5, but at a considerably stronger shock: The specimen thickness is 6.370 mm, impact velocity is 1.567 km/s, and peak stress is 30.4 GPa. Calculations with $\tau=15$ and 30 ns are compared with VISAR data in Fig. 9, and we conclude that τ around 20 ns would give the best agreement with experiment for the $P2$ rise time. When the parameter A_R is varied between 0 and 419 J/mol, the range which brackets the optimal value for experiment 5, the effect on the PIR is barely perceptible. This is because the phase interface is quite weak in experiment 6, with λ changing only from 0.90 to 0.99 across the phase interface.

Experiment 7 of Barker and Hollenbach is a thick-specimen copy of experiment 5: The specimen thickness is 19.14 mm, impact velocity is 1.292 km/s, and peak stress is 23.7 GPa. Calculations are compared with VISAR data in Fig. 10 with $\tau=30$ and 60 ns and $A_R=0$ J/mol, and in Fig. 11 with $\tau=60$ ns and $A_R=0$ and 419 J/mol. These parameter values bracket the best agreement with experiment for the $P2$ and PIR waves; our estimate for best values is τ around 50 ns and A_R around 200 J/mol.

An important property of our calculations is that the $P2$ wave becomes steady, with a constant rise time, in a time of around 6τ after impact. This result has implications for linear relaxation. For while τ can vary with shock strength, τ should be essentially the same for experiments 5 and 7, which differ only in specimen thickness. For values of τ which fit the $P2$ rise times of experiments 5 and 7, i.e., $\tau\approx30$–50 ns, our calculations produce $P2$ waves which are steady after, say, 0.3 μs. On the other hand, our interpretation of the VISAR data is that $P2$ is probably steady after 4 μs, experiment 7, but is definitely not steady after 1 μs, experiment 5. The implication is that, while linear relaxation might be an acceptable first approximation, some nonlinear relaxation is definitely present in the shock process.

The Barker-Hollenbach experiments which exhibit $P2$ waves range in peak stress from 17.3 to 30.4 GPa. We have compared calculations with measurements for experiments at 23.6, 23.7, and 30.4 GPa, and from these comparisons we have learned what the profiles tell us about the parameters τ, A_R, and B_R. As a final test of our modeling, we study experiment 1, which has a specimen thickness of 6.317 mm, impact velocity of 0.9916 km/s, and peak stress 17.3 GPa. The parameters were set as follows: $\tau=36$ ns, a little larger than our approximate steady-wave result from Sec. IV (see Table III); $A_R=0$ from our PIR analysis of this section; and

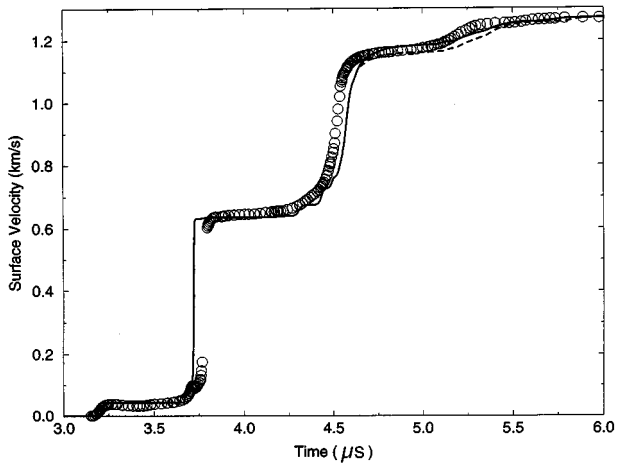

FIG. 11. Free surface velocity vs time for experiment 7 of Barker and Hollenbach (Ref. 5) (circles), compared with calculations at $\tau=60$ ns for $A_R=0$ (solid line) and $A_R=419$ J/mol (dashed line).

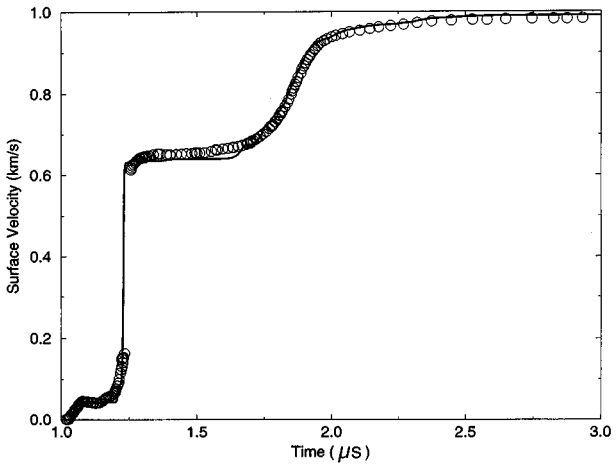

FIG. 12. Free surface velocity vs time for experiment 1 of Barker and Hollenbach (Ref. 5) (circles), compared with our calculation (solid line).

$B_R=642$ J/mol, as always. The overall agreement of our calculation with VISAR data is excellent, as shown in Fig. 12.

VI. SUMMARY AND CONCLUSIONS

A. Metastability

The equilibrium surface for a mixture of α and ε iron is defined by $\Delta G=0$, where $\Delta G=G_\alpha-G_\varepsilon$. As demonstrated by Andrews[3] and as shown here in Fig. 2, the iron Hugoniot does not lie on the equilibrium surface, but lies instead on a metastable surface, whose lifetime must be long compared to the microsecond time scale of the shock experiments. The value of λ on the metastable surface is denoted λ_m, and because of hysteresis, the metastable surfaces for forward and reverse transitions are separated. For both forward and reverse transitions, we propose that the metastable surface is determined by a balance between the thermodynamic driving force ΔG and an opposing force resulting from the buildup of stresses as the transition proceeds, implying $d\lambda_m \propto d\Delta G$. Further, $d\lambda_m$ should be proportional to the amount of the transforming phase present, i.e., $d\lambda_m \propto 1-\lambda_m$ for the forward transition and $d\lambda_m \propto \lambda_m$ for the reverse transition. These expressions for $d\lambda_m$ integrate to Eq. (15) for the forward transition surface and Eq. (21) for the reverse transition surface. We note the form of Eq. (15) was found empirically by Forbes[4] by fitting Hugoniot data.

The forward transition metastable surface can be made to fit Hugoniot data quite well in the mixed-phase region, as shown in Fig. 2, indicating that the form (15) is qualitatively correct. Figure 2 also indicates that our theoretical thermodynamic functions for α and ε iron are quite accurate in the region of the Hugoniot. While the shock experiments give no direct information on the shape of the reverse transition metastable surface, we were able to calibrate the proposed form (21) through its sensitivity to the arrival time and shape of the PIR. Results of these metastable surface calibrations are as follows.

(a) $A_F=0$ implies the shock-induced transition begins at the equilibrium phase boundary, specifically at $\sigma=13.22$ GPa and $T=350$ K on the Hugoniot (see Table II), corresponding to $P=13.0$ GPa at $T=300$ K.

(b) $B_F=B_R=642$ J/mol is the energy scale of forces opposing the transition. Dividing by $\Delta V=V_\alpha-V_\varepsilon$ yields 2 GPa for an estimate of the magnitude of the stresses involved.

(c) $A_R/B_R=0\rightarrow0.65$ implies that the reverse transition begins at $P=13\rightarrow11.8$ GPa at 300 K.

Our shock-calibrated metastable surfaces are compared in Fig. 3 with room-temperature hydrostatic diamond-cell measurements of Taylor *et al.*[31] The agreement for the forward transition is striking, implying that both the shock-induced and quasistatic transitions proceed on the same metastable surface. Further, our reverse transition surface is in qualitative agreement with the diamond-cell data, though we are clearly missing a small amount of early retransformation from ε to α.

B. Dynamics

In Sec. IV we noted that decay of the $P1$ wave is only weakly dependent on the relaxation time τ and, hence, does not provide a sensitive way to determine τ. We then carried out an approximate steady-wave analysis of the $P2$ rise time, and using the Barker-Hollenbach[5] data, we found values of τ in the range 12–60 ns, depending mainly on the shock strength (Fig. 5). However, Fig. 5 also shows a small but definite dependence of τ on specimen thickness, apparently related to the fact that $P2$ waves are not yet steady for the thin specimens (Fig. 4). We therefore carried out numerical calculations of impact experiments, accounting for the complete (nonsteady) wave evolution process, but retaining the linear relaxation description of the phase transition rate, given by Eq. (17). Results of these numerical calculations are as follows.

(a) From our theoretical thermodynamic functions for α and ε iron, together with the properly adjusted relaxation time and reverse transition parameters, calculated free surface wave profiles are in excellent overall agreement with VISAR data (except for the $P1$ wave front, where our lack of rate-dependent plasticity is apparent). The comparisons are shown in Figs. 6–12.

(b) The relaxation times were determined by fitting to the $P2$ rise times and show substantial agreement with the approximate steady-wave analysis of Sec. IV.

(c) The $P2$ wave becomes steady by a time of approximately 6τ after impact.

This last result has a significant consequence. Since τ can depend on P and T, τ can vary with shock strength, but τ should be essentially the same for experiments at a common shock strength. Hence experiments 5 and 7 should have the same τ, and our calculations indicate that both experiments should exhibit steady $P2$ waves, with a constant rise time, a result inconsistent with the data of Barker and Hollenbach. We therefore conclude, at the highest level of accuracy of the VISAR measurements, corresponding to an accuracy within 10% for the $P2$ rise times, that some nonlinear relaxation is present in the shock process.

ACKNOWLEDGMENTS

We are indebted to L. M. Barker and R. D. Taylor for providing data from Refs. 5 and 31 in tabular form. This work was supported by the U. S. Department of Energy.

[1] S. Minshall, Phys. Rev. **98**, 271 (1955).
[2] D. Bancroft, E. L. Peterson, and S. Minshall, J. Appl. Phys. **27**, 291 (1956).
[3] D. J. Andrews, J. Phys. Chem. Solids **34**, 825 (1973).
[4] J. W. Forbes, Experimental Investigation of the Kinetics of Shock-Induced Alpha to Epsilon Phase Transition in Armco Iron (Washington State University Report WSU-SDL 76-01, Pullman, Washington, 1976).
[5] L. M. Barker and R. E. Hollenbach, J. Appl. Phys. **45**, 4872 (1974).
[6] G. E. Duvall and R. A. Graham, Rev. Mod. Phys. **49**, 523 (1977).
[7] D. C. Wallace, *Thermodynamics of Crystals* (Wiley, New York, 1972).
[8] R. E. Swanson, G. K. Straub, B. L. Holian, and D. C. Wallace, Phys. Rev. B **25**, 7807 (1982).
[9] G. K. Straub and D. C. Wallace, Phys. Rev. B **30**, 3929 (1984).
[10] D. C. Wallace, Proc. R. Soc. London Ser. A **433**, 631 (1991).
[11] D. C. Wallace, Proc. R. Soc. London Ser. A **439**, 177 (1992).
[12] D. C. Wallace, Phys. Rev. B **46**, 5242 (1992).
[13] O. Eriksson, J. M. Wills, and D. C. Wallace, Phys. Rev. B **46**, 5221 (1992).
[14] G. K. Straub, J. B. Aidun, J. M. Wills, C. R. Sanchez-Castro, and D. C. Wallace, Phys. Rev. B **50**, 5055 (1994).
[15] C. Kittel, *Solid State Physics*, 5th ed. (Wiley, New York, 1976), p. 167.
[16] D. A. Boness, J. M. Brown, and A. K. McMahan, Phys. Earth Planet. Inter. **42**, 227 (1986).
[17] J. M. Leger, C. Loriers-Susse, and B. Vodar, Phys. Rev. B **6**, 4250 (1972).
[18] H. K. Mao, W. A. Bassett, and T. Takahashi, J. Appl. Phys. **38**, 272 (1967).
[19] H. K. Mao, Y. Wu, L. C. Chen, and J. F. Shu, J. Geophys. Res. **95**, 21737 (1990).
[20] J. C. Boettger and S. B. Trickey, Phys. Rev. B **53**, 3007 (1996); see also G. K. Straub and J. M. Wills (unpublished).
[21] P. Vinet, J. Ferrante, J. H. Rose, and J. R. Smith, J. Phys. Condens. Matter **1**, 1941 (1989).
[22] A. F. Guillermet and P. Gustafson, High Temp.-High Press. **16**, 591 (1985).
[23] F. P. Bundy, J. Appl. Phys. **36**, 616 (1965).
[24] L. Kaufman, E. V. Clougherty, and R. J. Weiss, Acta Metall. **11**, 323 (1963).
[25] P. C. Johnson, B. A. Stein, and R. S. Davis, J. Appl. Phys. **33**, 557 (1962).
[26] In our notation, the difference between normal and transverse compressive stresses at yield is $2y$; for a comparison of different measures of yield strength, see D. C. Wallace, Thermoelastic-Plastic Flow in Solids (LA-10119, Los Alamos National Laboratory, Los Alamos, New Mexico, 1985).
[27] J. C. Boettger, J. Appl. Phys. **72**, 5500 (1992).
[28] J. C. Boettger, M. D. Furnish, T. N. Dey, and D. E. Grady, J. Appl. Phys. **78**, 5155 (1995).
[29] W. A. Bassett and E. Huang, Science **238**, 780 (1987).
[30] N. von Bargen and R. Boehler, High Press. Res. **6**, 133 (1990).
[31] R. D. Taylor, M. P. Pasternak, and R. Jeanloz, J. Appl. Phys. **69**, 6126 (1991).
[32] L. M. Barker, J. Appl. Phys. **46**, 2544 (1975).
[33] Y. Horie and G. E. Duvall, Shock Waves and the Kinetics of Solid-S Transitions (Washington State University Report WSU-SDL 68-06, Pullman, Washington, 1968).
[34] J. N. Johnson, in *High-Pressure Shock Compression of Solids*, edited by J. R. Asay and M. Shahinpoor (Springer-Verlag, New York, 1993), p. 217.
[35] R. I. Nigmatulin, Zh. Prikl. Mekh. Tekh. Fiz. **1**, 88 (1970).
[36] S. S. Grigorian, K. A. Kozorezov, R. I. Nigmatulin, N. F. Skugorova, and N. N. Kholin, Astron. Acta **17**, 405 (1972).
[37] N. K. Akhmadeev and R. I. Nigmatulin, Zh. Prikl. Mekh. Tekh. Fiz. **5**, 128 (1976).
[38] N. K. Akhmadeev, N. A. Akhmetova, and R. I. Nigmatulin, Zh. Prikl. Mekh. Tekh. Fiz. **6**, 113 (1984).